Wind and Structures, Vol. 15, No. 5 (2012) 441-462
DOI: http://dx.doi.org/10.12989/was.2012.15.5.441

Limitations for the control of wind-loaded slender bridges with movable flaps

Arno Kirch* and Udo Peil

Institute of Steel Structures, Technische Universität Carolo-Wilhelmina zu Braunschweig, Beethovenstrasse 51, 38106 Braunschweig, Germany

(Received July 12, 2010, Revised December 20, 2010, Accepted March 13, 2012)

Abstract. This article presents theoretical investigations on techniques for the improvement of the dynamic characteristics of slender bridges under wind action. Aerodynamically effective control shields are applied as controlled actuators. The first part of the article describes the modelling of the uncontrolled aeroelastic system. Acting aerodynamic forces are consistently characterised using linear time-invariant transfer elements in terms of rational functions. On this basis, two configuration levels of the uncontrolled system are represented with linear time-invariant state-space models and investigated. The second part of the article addresses controller design and the behaviour of the controlled aeroelastic system. Both fundamental limits for stabilisation and the efficiency for attenuating the influence of gusts are described for different actuator mechanisms. The results are derived and discussed with methods of control theory.

Keywords: bridges; state-space model; flutter; divergence; active aerodynamic control

1. Introduction

In recent years, a number of techniques have been investigated to improve the vibration behaviour of bridges especially under wind action by systematically imposing additional forces. They should reduce the system deflection due to wind action and avoid the occurrence of aeroelastic instabilities.

This article addresses damping and stabilisation of an aeroelastic system with additional aerodynamic forces. The forces are generated with rotating control shields that are connected with the bridge girder. In contrast to actuators like reaction wheels or gyroscopes, which affect the bridge with inertial or gyroscopic forces (Kirch and Peil 2009), not only the flutter but also the divergence wind speed of the system can be modified. Moreover, control shields need no minimum mass and, hence, they only marginally increase the self-weight of the bridge. The forces that are transmitted from the control shields to the bridge girder are generated by the air flow. Assuming a proper design, it can be expected that considerably lower forces are thus necessary for the control of the shields compared to the control of the other mentioned kinds of actuators.

Aerodynamically effective, movable control surfaces have been used in aerospace engineering for many years to suppress the influences of disturbances on aircraft wings (e.g., Edwards 1977). Their application to bridge decks was proposed for instance in Klein *et al*. (1972). It was investigated in Kobayashi and Nagaoka (1992) and Ostenfeld and Larsen (1992) for the first time. In aerospace

* Corresponding author, E-mail: a.kirch@is.tu-braunschweig.de

engineering, the primary task of a wing is to produce a lifting force. Flaps as integrated parts of the aerofoil modify its surface in order to evoke positive effects without increasing the disturbing impact of gusts. With respect to bridges, however, control shields are extra components that augment the area exposed to the wind. The shields cannot bear any significant live load and can hence not directly fulfil the intrinsic task of a bridge. In addition to motion-induced aerodynamic forces, new gust-induced forces arise simultaneously, which also need to be suppressed. Therefore, aerodynamically effective control shields are generally less effective for bridges than for aircraft wings. Moreover, control shields need a minimum wind speed to work. They are not suited for damping oscillations in still air. This shortcoming is similar to that of fin stabilisers, which are used to counteract the rolling of ships. Aircraft wings do not possess this disadvantage either.

Here, the theoretically investigated two-dimensional bridge-like system is equipped with aerodynamically balanced flaps. They are attached to both sides of the bridge girder (Fig. 1) and actively controlled. In contrast to control shields that are located far away from the bridge girder, adjacent flaps can modify the flow around the girder effectively and favourably. This article presents new insights into fundamental stabilisation limits and the ability of gust alleviation, which are derived with mathematically consistent, correct models and tools. Similar systems with actively controlled shields have been investigated in several journal articles and dissertations (Kwon 1996, Preidikman and Mook 1997, Hansen 1998, Wilde and Fujino 1998, Cobo del Arco and Aparicio 1999, Piésold and Corney 1999, Hansen *et al*. 2000, Huynh 2000, Kwon and Chang 2000, Hansen and Thoft-Christensen 2001, Huynh and Thoft-Christensen 2001, Wilde *et al*. 2001, Nissen *et al*. 2004). In addition, a number of conference papers that are written by the same authors are available. For the sake of completeness, it should be noted that investigations on passively controlled bridges with aerodynamically effective appendages have been published as well (e.g., Preidikman and Mook 1998, Wilde *et al*. 1999, Omenzetter *et al*. 2000a,b, Omenzetter *et al*. 2002a,b, Aslan and Starossek 2008).

2. State-space model and open-loop characteristics of the aeroelastic system

2.1. Aerodynamic forces

In order to investigate an aerodynamically controlled bridge system with methods of control theory, a realistic and mathematically consistent description of the forces caused by the wind flow around the girder is of particular importance. Usually, wind action is divided into several types of wind loads.

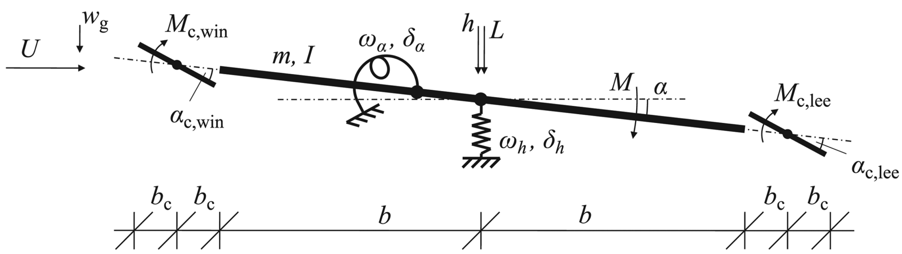

Fig. 1 Two-dimensional aeroelastic system with four aerodynamically effective degrees of freedom

Along with its structural parameters, motion-induced wind forces influence the properties of an aeroelastic system. For an adequate representation of the displacement-force relation, a transfer equation with a linear time-invariant transfer element is used (e.g., Kirch and Peil 2011).

$$\mathbf{f}(p) = \mathbf{G}(p) \cdot \xi_s(p) \tag{1}$$

The variable $\mathbf{G}$ represents the aerodynamic transfer function that is here alternatively termed aerodynamic admittance. In Eq. (1), the aerodynamic force vector is denoted by $\mathbf{f}$, while the vector of the aerodynamically effective degrees of freedom is denoted by ξ_s. In this pure frequency-domain description, the values are to be regarded as unilateral Laplace transforms. The variable in the frequency domain p is the reduced complex frequency.

$$p = sb/U = (\sigma + \mathrm{i}\omega)b/U = \beta + \mathrm{i}k \tag{2}$$

The complex, non-reduced frequency is symbolised by s, b stands for the half width of the primary bridge cross section according to the system shown in Fig. 1, and U symbolises the constant horizontal mean wind speed. The following notation according to Küssner and Schwarz (1940) has been used in aerospace engineering since early publications on aerodynamics. A factor q_0, which includes the air density ρ, is usually separated from the transfer function of motion-induced forces.

$$\mathbf{f}(p) = q_0 \cdot \mathbf{Q}(p) \cdot \xi_s(p), \quad q_0 = \pi\rho b^2 U^2 \tag{3}$$

Thus, the matrix $\mathbf{Q}$ is only a function of the reduced complex frequency p. Its elements are called aerodynamic derivatives. For the two-dimensional example displayed above, the theoretical derivatives based on potential theory are used as proposed in Küssner and Göllnitz (1964) according to Küssner and Schwarz (1940). In the mentioned references, the results are derived for a wing-aileron-tab combination, which is typical of aerospace engineering. The geometry and the derivatives of the airfoil can be linearly transformed into the corresponding properties of the system shown in Fig. 1. Transformation details are not listed here. Bridges with aerodynamically effective flaps are assumed to have streamlined cross sections. Therefore the derivatives of the bridge-flap system are similar to the ones of the flat-plate combination based on potential theory. In contrast to the aerodynamic forces derived in Theodorsen and Garrick (1941), which are used in many publications on aerodynamic control of bridges, the case of open gaps between the airfoil components is additionally considered in Küssner and Göllnitz (1964). The flow through these gaps is taken into account in the formulas of the corresponding forces. This approach is used here.

The motion-induced aerodynamic forces of the aeroelastic system with four aerodynamically effective degrees of freedom shown in Fig. 1 can be described with the following detailed equation.

$$(Lb \;\; M \;\; M_{c,\mathrm{win}} \;\; M_{c,\mathrm{lee}})^{\mathrm{T}}_{(p)} = q_0 \cdot (Q_{jl})_{(p)} \cdot (h/b \quad \alpha \quad \alpha_{c,\mathrm{win}} \quad \alpha_{c,\mathrm{lee}})^{\mathrm{T}}_{(p)}, \; j,l = 1, \ldots, 4 \tag{4}$$

Forces that act on the total aerodynamically effective cross section are denoted by L and M. The moments $M_{c,\mathrm{win}}$ and $M_{c,\mathrm{lee}}$ act on the flaps around their hinges. A dimensionless $\mathbf{Q}$ matrix is obtained when using identical dimensions for both the different types of deformations and the different types of loads. For the investigations presented here, the half width of the flaps is set to $b_c = 0.1\ b$. As can be seen in Fig. 1, the flap hinges, which are fixed relative to the bridge girder, are located at the middle of the flaps. The derivatives of the bridge cross section without flaps correspond to the submatrix of $\mathbf{Q}$ in Eq. (4) for $j,l = 1,\ldots,2$ and $b_c = 0$. For purely imaginary frequencies $p = 0+\mathrm{i}k$, the conversion to Scanlan derivatives (Simiu and Scanlan 1996), which are often used in bridge engineering, can be taken from Kirch and Peil (2009), for instance.

Gusts act on girder and flaps. Similar to Eq. (1), gust-induced forces $\mathbf{d}^{\mathrm{g}}$ – also called buffeting forces – which constitute another type of wind forces, can be related to zero-mean fluctuating velocity components of gusts α_{g} with aerodynamic gust admittances $\mathbf{G}^{\mathrm{g}}$.

$$\mathbf{d}^{\mathrm{g}}(p) = \mathbf{G}^{\mathrm{g}}(p) \cdot \alpha_{\mathrm{g}}(p) = q_0 \cdot \mathbf{Q}^{\mathrm{g}}(p) \cdot \alpha_{\mathrm{g}}(p) \tag{5}$$

For the system given in Fig. 1, according to the potential theory (Sears 1940), the vector of the dimensionless gust speeds contains one element only, the dimensionless vertical gust speed $\alpha_{\mathrm{g}} = w_{\mathrm{g}}/U$. Forces due to flow separation and vortex shedding are not considered here. They are assumed to be negligible for the streamlined cross section investigated here.

Usually, analytic functions of the complex frequency are taken to express the transfer function of motion-induced aerodynamic forces. With the aid of these functions, the derivatives of bridge cross sections, which are available for harmonic oscillations, are approximated. Rational functions are the most commonly used analytic transfer function approximations in aerospace engineering as well as in bridge engineering. In this article, rational functions according to the Minimum-State Method (Karpel 1981) are used.

$$\mathbf{Q}(p) = \mathbf{A}_0 + \mathbf{A}_1 p + \mathbf{A}_2 p^2 + \mathbf{D}(p\mathbf{I} - \mathbf{R})^{-1}\mathbf{E}p, \quad \mathbf{R} = -\mathrm{diag}(\gamma_1, \gamma_2, \ldots, \gamma_{n_{\mathrm{L}}}) \tag{6}$$

This approach is based on rational transfer functions with single, real poles $(-\gamma_l)$, which are the same for all derivatives. Rational functions are particularly suitable for approximating the aerodynamic derivatives of girders with streamlined cross sections not only along the imaginary axis but also in other important areas of the complex frequency plane (Kirch and Peil 2011). The constant matrices $\mathbf{A}_1$, $\mathbf{A}_2$, $\mathbf{D}$, $\mathbf{E}$ and $\mathbf{R}$ are determined with elaborate approximation procedures according to Tiffany Hoadley and Adams (1988). For the following examples, the derivative approximation is carried out with $n_{\mathrm{L}} = 5$ poles. Steady values of the derivatives are incorporated in the $\mathbf{A}_0$ matrix. Exact matching of the steady values is important for the evaluation of the divergence wind speed. In Eq. (6), the parameter b_c is no longer accessible. Hence, the derivatives for the flap-free case cannot be obtained as a submatrix of the case with flaps. The approximation is thus separately carried out for the cross section with and without flaps. As described for motion-induced forces, the approximation of the gust admittance can be performed as well. Separated from the derivatives, it is approximated with its own poles.

2.2. State-space model and characteristics of the aeroelastic system without flaps

After inserting Eq. (6) into Eq. (3), a part of the last summand of the resulting equation can be transformed into a linear differential equation with constant coefficients by introducing artificial so-called aerodynamic lag states ξ_{a}.

$$\xi_{\mathrm{a}} = (p\mathbf{I} - \mathbf{R})^{-1}\mathbf{E}p\xi_{\mathrm{s}} \;\bullet\!\!-\!\!\circ\; \xi_{\mathrm{a}}' - \mathbf{R}\xi_{\mathrm{a}} = \mathbf{E}\xi_{\mathrm{s}}' \tag{7}$$

The symbol between the equations connects corresponding frequency and time-domain descriptions assuming that the values of all time-dependent functions are zero prior to time $t = 0$. The prime $(\,)'$ symbolises the generalised differentiation with respect to the non-dimensionalised time $\bar{t}$.

$$\bar{t} = (U/b)t \tag{8}$$

Together with a linear structure description of the same kind

$$\mathbf{M}_s\ddot{\xi}_s + \mathbf{C}_s\dot{\xi}_s + \mathbf{K}_s\xi_s = \mathbf{f} + \mathbf{u} + \mathbf{d}^g + \mathbf{d}^g \tag{9}$$

the aeroelastic system can be represented by a linear time-invariant state-space model

$$\dot{\mathbf{x}} = \mathbf{A}\mathbf{x} + \mathbf{B}\mathbf{u} + \mathbf{E}^g\mathbf{d}^g + \mathbf{E}^d\mathbf{d}^d \tag{10a}$$

$$\mathbf{y} = \mathbf{C}\mathbf{x} \tag{10b}$$

where $\mathbf{x}$ is the state vector and $(\dot{\ })$ symbolises the generalised differentiation with respect to time t.

$$\mathbf{x} = (\dot{\xi}_s^T \;\; \xi_s^T \;\; \xi_a^T)^T \tag{11}$$

The matrices of the structural variables mass, damping and stiffness are denoted in these equations by $\mathbf{M}_s$, $\mathbf{C}_s$ and $\mathbf{K}_s$ respectively. $\mathbf{A}$ is the system matrix

$$\mathbf{A} = \begin{pmatrix} -\overline{\mathbf{M}}^{-1}\overline{\mathbf{C}} & -\overline{\mathbf{M}}^{-1}\overline{\mathbf{K}} & q_0\overline{\mathbf{M}}^{-1}\overline{\mathbf{D}} \\ \mathbf{I} & \mathbf{0} & \mathbf{0} \\ \mathbf{E} & \mathbf{0} & (U/b)\mathbf{R} \end{pmatrix} \tag{12}$$

where

$$\overline{\mathbf{M}} = \mathbf{M}_s - q_0(b/U)^2\mathbf{A}_2, \quad \overline{\mathbf{C}} = \mathbf{C}_s - q_0(b/U)\mathbf{A}_1, \quad \overline{\mathbf{K}} = \mathbf{K}_s - q_0\mathbf{A}_0\,. \tag{13}$$

In the state Eq. (10(a)) $\mathbf{d}^d$ represents other disturbance forces originating from traffic for instance. The control input $\mathbf{u}$ is important for closed-loop control, and is to be regarded in this section as external forces, which correspond to the structural degrees of freedom. The input matrices $\mathbf{B}$, $\mathbf{E}^g$ and $\mathbf{E}^d$ of the control input and the disturbances have the same entries.

$$\mathbf{B} = \mathbf{E}^g = \mathbf{E}^d = ((\overline{\mathbf{M}}^{-1})^T \quad \mathbf{0}^T \quad \mathbf{0}^T)^T \tag{14}$$

The output equation Eq. (10(b)) cannot extract more than the structural states $\dot{\xi}_s, \xi_s$. In reality, the mathematically introduced lag states ξ_a cannot be measured. The mean horizontal wind speed U occurs in the system matrix $\mathbf{A}$ as a parameter.

The dynamic characteristics of the aeroelastic system can be evaluated with an eigenvalue analysis of the system matrix $\mathbf{A}$. System stability is of major interest in this context. Due to the effect of motion-induced aerodynamic forces, aeroelastic instabilities can occur in the form of flutter and divergence. Unless otherwise explained, the two terms should specifically denote the cases when the system is Lyapunov stable but not asymptotically stable. Since the system matrix contains the mean

Table 1. Structural properties of the two-dimensional aeroelastic model

half deck width	b= 15.0 m
mass	m= 25.0·10^3 kg/m
moment of inertia	I= 2.80·10^6 kgm^2/m
eigenfrequencies	ω_h= 0.628 1/s
$k_h = \omega_h^2\, m$; $k_\alpha = \omega_\alpha^2\, I$	ω_α= 1.13 1/s
logarithmic damping decrements	δ_h= 0.0126
$c_h = \delta_h\, m\, \omega_h/\pi$; $c_\alpha = \delta_\alpha\, I\, \omega_\alpha/\pi$	δ_α= 0.0126

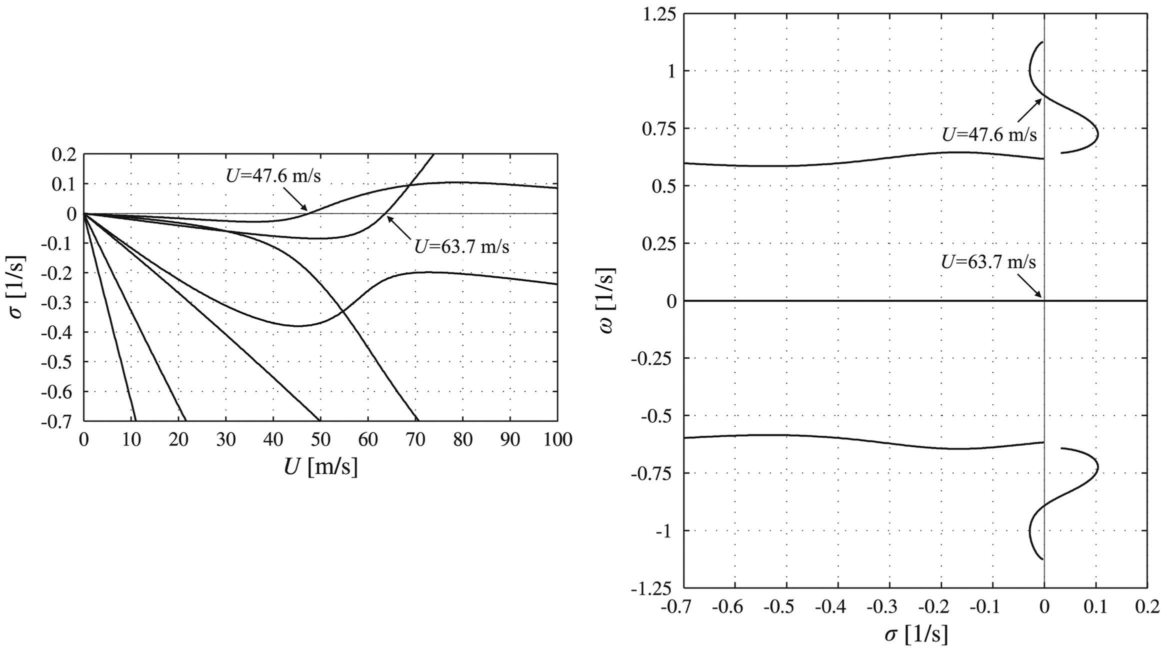

Fig. 2 Eigenvalues of the aeroelastic system without flaps

horizontal wind speed U, a parameter-dependent linear eigenvalue problem must be solved.

The two-dimensional, generalised system in Fig. 1 is used as an example with the characteristic structural properties given in Table 1. The corresponding structural matrices are as follows.

$$\mathbf{M}_\mathrm{s} = \begin{pmatrix} mb^2 & 0 \\ 0 & I \end{pmatrix}, \qquad \mathbf{C}_\mathrm{s} = \begin{pmatrix} c_h b^2 & 0 \\ 0 & c_\alpha \end{pmatrix}, \qquad \mathbf{K}_\mathrm{s} = \begin{pmatrix} k_h b^2 & 0 \\ 0 & k_\alpha \end{pmatrix} \tag{15}$$

At the zero crossings of the eigenvalue real-part curves (Fig. 2), flutter appears at $U = 47.6$ m/s and divergence at $U = 63.7$ m/s . This identification is possible when inspecting the eigenvalues and state eigenvectors. Flutter occurs in two complex-conjugate eigenvectors with complex values. Its eigenfrequencies are purely imaginary and complex conjugate. In the case of the flat plate, both structural degrees of freedom appear in the same order of magnitude, as can be predicted for the classical bending-torsional flutter. Divergence has only one eigenvector, the element values of which are real and vanish in the velocities ξ_s and in the lag states ξ_a. Its eigenfrequency is zero. In the case of uncontrolled bridges, the divergence wind speed is usually higher than the flutter wind speed and therefore normally not the focus of interest. This statement cannot be held up when actuators are applied. The sections in the second part of the article explain how and within what limits the system characteristics can be changed.

2.3 State-space model and open-loop characteristics of the aeroelastic system extended with flaps

The mathematical description of the flap-extended aeroelastic system depends on the type of the chosen control input. One possibility is to act on the extended aeroelastic system through forces in the form of torques around the flap hinges. In this article it is assumed that there is no passive coupling by devices like springs or dampers between the rotation of the flaps and the bridge girder. In addition to inertial forces, which arise when accelerating the flaps, the input forces are thus buffered by motion-induced aerodynamic forces only. This usually leads to very non-robust controllers and, together with other reasons, to various numerical problems. The situation becomes worse if the flaps are modelled without a mass. This is done here in order to investigate the purely aerodynamic effectiveness of flaps. The self-weight of the bridge should not unnecessarily increase due to attached flaps. Hence, a lightweight construction is preferable and a massless modelling of the flaps is not unrealistic.

If a control input is chosen in the form of displacements, the mentioned numerical problems are circumvented. For the derivation of the motion equations of an aeroelastic system with flaps and displacement input, the following procedure is recommendable. In the transfer equations of aerodynamic forces and in the transfer matrices of Section 2.1 only those rows are considered that correspond to forces acting on the total aerodynamically effective system. Accordingly, in the approximation matrices $\mathbf{A}_j$ and $\mathbf{D}$ the other rows must be cancelled. The aerodynamically effective degrees of freedom can be separated. One part still corresponds to the structural degrees of freedom $\xi_s = (h/b \quad \alpha)^T$. The other part represents the displacement inputs ξ_c , which, in the example of Fig. 1, include the relative flap angles $\alpha_{c,win}$ and $\alpha_{c,lee}$. The derivatives can be separated as well.

$$\mathbf{f} = q_0(\mathbf{Q}^s \quad \mathbf{Q}^c)(\xi_s^T \quad \xi_c^T)^T = q_0\mathbf{Q}^s\xi_s + q_0\mathbf{Q}^c\xi_c \tag{16}$$

Motion-induced aerodynamic forces are thus assigned to their different origins. Correspondingly, the approximation matrices must be separated or remain unchanged.

$$\mathbf{A}_j = (\mathbf{A}_j^s \quad \mathbf{A}_j^c), \qquad \mathbf{E} = (\mathbf{E}^s \quad \mathbf{E}^c), \qquad \mathbf{D} = \mathbf{D}^s = \mathbf{D}^c, \qquad \mathbf{R} = \mathbf{R}^s = \mathbf{R}^c \tag{17}$$

The transfer from displacement inputs ξ_c to control forces $\mathbf{u}$, which act on the total aerodynamic cross section, can be described with a state-space model

$$\dot{\xi}_a^c = \mathbf{A}_c\xi_a^c + \mathbf{B}_c\mathbf{x}_c \tag{18a}$$

$$\mathbf{u} = \mathbf{C}_c\xi_a^c + \mathbf{D}_c\mathbf{x}_c \tag{18b}$$

where

$$\mathbf{x}_{\mathrm{c}} = (\ddot{\xi}_{\mathrm{c}}^{\mathrm{T}} \quad \dot{\xi}_{\mathrm{c}}^{\mathrm{T}} \quad \xi_{\mathrm{c}}^{\mathrm{T}})^{\mathrm{T}}. \tag{19}$$

The matrices of the state-space model can be derived from the approximation matrices of Eq. (17) as follows.

$$\mathbf{A}_{\mathrm{c}} = \frac{U}{b}\mathbf{R}^{\mathrm{c}}, \quad \mathbf{B}_{\mathrm{c}} = (\mathbf{0} \quad \mathbf{E}^{\mathrm{c}} \quad \mathbf{0}), \quad \mathbf{C}_{\mathrm{c}} = q_0\mathbf{D}^{\mathrm{c}}, \quad \mathbf{D}_{\mathrm{c}} = q_0\left(\left(\frac{b}{U}\right)^2\mathbf{A}_2^{\mathrm{c}} \ \frac{b}{U}\mathbf{A}_1^{\mathrm{c}} \ \mathbf{A}_0^{\mathrm{c}}\right) \tag{20}$$

The equations of motion of the flap-extended aeroelastic system comply in their form with Eq. (9). When applying flaps without a mass, the structural matrices $\mathbf{M}_{\mathrm{s}}$, $\mathbf{C}_{\mathrm{s}}$ and $\mathbf{K}_{\mathrm{s}}$ remain unchanged compared to Eq. (15). The forces on the right-hand side of Eq. (9) must be specified as explained in this section. As a consequence of separating the aerodynamically effective degrees of freedom, the approximation matrices $\mathbf{A}_j$ and $\mathbf{E}$ inside the system matrix $\mathbf{A}$ and the aerodynamic lag states ξ_{a} in the state vector $\boldsymbol{x}$ must be replaced by $\mathbf{A}_j$, $\mathbf{E}^{\mathrm{s}}$ and $\xi_{\mathrm{a}}^{\mathrm{s}}$, respectively.

Since the derivatives $\mathbf{Q}^{\mathrm{s}}$ und $\mathbf{Q}^{\mathrm{c}}$ are approximated simultaneously, the aerodynamic lag states can be added and a single new state ξ_{a} can be defined. If the summand $\mathbf{Bu}$ is replaced by $\tilde{\mathbf{B}}\mathbf{x}_{\mathrm{c}}$ where

$$\tilde{\mathbf{B}} = (\mathbf{B}\mathbf{D}_{\mathrm{c}}) + (\mathbf{0}^{\mathrm{T}} \quad \mathbf{B}_{\mathrm{c}}^{\mathrm{T}})^{\mathrm{T}}, \tag{21}$$

both state-space models can be combined into a single one with the following state equation.

$$\dot{\mathbf{x}} = \mathbf{A}\mathbf{x} + \tilde{\mathbf{B}}\mathbf{x}_{\mathrm{c}} + \mathbf{E}^{\mathrm{g}}\mathbf{d}^{\mathrm{g}} + \mathbf{E}^{\mathrm{d}}\mathbf{d}^{\mathrm{d}} \tag{22}$$

The state-space model can be easily modified with summands taking inertia effects of the flaps into account.

When extending the aeroelastic system with unmoved flaps, its eigenvalue curves are altered (Fig. 3). Since a larger area is exposed to the wind, the flutter wind speed decreases to $U = 43.5$ m/s and the divergence wind speed to $U = 53.1$ m/s. To systematically influence the extended aeroelastic system, the displacement inputs of the extended aeroelastic system must depend on its outputs or states. Hence, the control loop must be closed.

As a consequence of the rational function approximation, the vector $\mathbf{x}_{\mathrm{c}}$ contains not only the displacement inputs ξ_{c}, but also their derivatives $\dot{\xi}_{\mathrm{c}}$ and $\ddot{\xi}_{\mathrm{c}}$. These subvectors are not independent

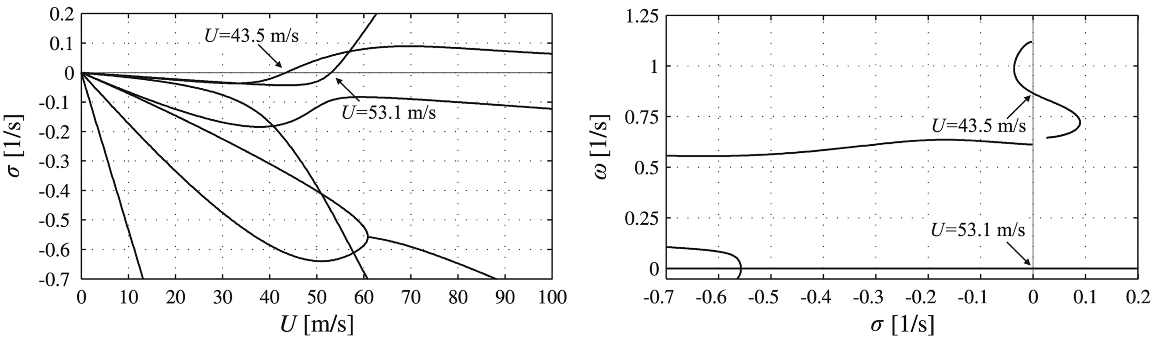

Fig. 3 Eigenvalues of the aeroelastic system with unmoved flaps

of one another and necessitate the application of an additional actuator model for the differentiation (ZAERO 2004) to allow the use of standard methods of control engineering. Hence, this actuator is at least mathematically motivated. For this purpose, a state-space model can be used that represents parallel third-order lag elements.

$$\dot{\mathbf{x}}_c = \mathbf{A}_{ac}\mathbf{x}_c + \mathbf{B}_{ac}\mathbf{u}_{ac} \tag{23}$$

$$\mathbf{A}_{ac} = \begin{pmatrix} -\mathbf{C}_a^2 & -\mathbf{C}_a^1 & -\mathbf{C}_a^0 \\ \mathbf{I} & \mathbf{0} & \mathbf{0} \\ \mathbf{0} & \mathbf{I} & \mathbf{0} \end{pmatrix}, \qquad \mathbf{B}_{ac} = \begin{pmatrix} \mathbf{C}_a^0 \\ \mathbf{0} \\ \mathbf{0} \end{pmatrix} \tag{24}$$

The submatrices only have nonzero entries on the main diagonal.

$$\mathbf{C}_a^j = \mathrm{diag}(c_{a,l}^j) \tag{25}$$

If the transient response is tuned to be sufficiently fast and non-oscillating, the input $\mathbf{u}_{ac}$ can be transferred to itself and its derivatives with sufficient precision. The transfer function from a single element of $\mathbf{u}_{ac}$ to the corresponding one of ξ_c is as follows.

$$\mathrm{G}_{ac,l}(s) = \frac{c_{a,l}^0}{s^3 + c_{a,l}^2 s^2 + c_{a,l}^1 s + c_{a,l}^0} = \frac{-s_1 s_2 s_3}{(s-s_1)(s-s_2)(s-s_3)} \tag{26}$$

In this article its poles are placed on the negative branch of the real axis at $s_1 = -100$ 1/s , $s_2 = -150$ 1/s and $s_3 = -200$ 1/s. Identical poles for different displacement inputs are unproblematic, because they are connected to different eigenvectors.

The model of the mathematical actuator in Eq. (23) can be combined with the state-space model of Eq. (22).

$$\begin{pmatrix} \dot{\mathbf{x}} \\ \dot{\mathbf{x}}_c \end{pmatrix} = \begin{pmatrix} \mathbf{A} & \tilde{\mathbf{B}} \\ \mathbf{0} & \mathbf{A}_{ac} \end{pmatrix}\begin{pmatrix} \mathbf{x} \\ \mathbf{x}_c \end{pmatrix} + \begin{pmatrix} \mathbf{0} \\ \mathbf{B}_{ac} \end{pmatrix}\mathbf{u}_{ac} + \begin{pmatrix} \mathbf{E}^g \\ \mathbf{0} \end{pmatrix}\mathbf{d}^g + \begin{pmatrix} \mathbf{E}^d \\ \mathbf{0} \end{pmatrix}\mathbf{d}^d \tag{27a}$$

$$\mathbf{y} = (\mathbf{C} \quad \mathbf{0})\begin{pmatrix} \mathbf{x} \\ \mathbf{x}_c \end{pmatrix} \tag{27b}$$

The block triangular form of the system matrix in Eq. (27(a)) shows that the eigenvalue curves described above are not affected by the dynamics of the mathematical actuator. To keep the eigenvalues of the mathematical actuator out of the closed loop, a state transformation into the canonical form is performed. In the canonical state space, these actuator eigenvalues can be separated.

The dynamic behaviour of sensors and other actuators is neglected in this article. They are assumed to be fast compared to the components of the extended aeroelastic system that are investigated here. With linear relations, the displacement inputs can be kinematically coupled to one another. For the numerical example, three different cases are considered: separately driven flaps, flaps rotated in opposite directions ($\alpha_c = -\alpha_{c,lee} = \alpha_{c,win}$) and flaps rotated in the same direction ($\alpha_c = \alpha_{c,lee} = \alpha_{c,win}$) . The first two cases require information about the flow direction.

Basis for the following investigations is the state-space model of Eq. (27). Its abbreviated state equation and output equation are as follows.

$$\dot{\mathbf{x}}_{\text{ol}} = \mathbf{A}_{\text{ol}}\mathbf{x}_{\text{ol}} + \mathbf{B}_{\text{ol}}\mathbf{u}_{\text{ac}} + \mathbf{E}_{\text{ol}}^{\text{g}}\mathbf{d}^{\text{g}} + \mathbf{E}_{\text{ol}}^{\text{d}}\mathbf{d}^{\text{d}} \tag{28a}$$

$$\mathbf{y} = \mathbf{C}_{\text{ol}}\mathbf{x}_{\text{ol}} \tag{28b}$$

By comparing these equations with Eq. (27), the definition of the introduced vectors and matrices can be found.

The following sections of the second part of this article describe how and within what limits the open-loop characteristics of the aeroelastic system can be changed with controlled motions of the aerodynamically effective flaps. The used methods are standard procedures in control engineering and described in books on principles of control theory. For this article, the authors have worked mainly with the textbooks Lunze (2004, 2005).

3. Controller design

3.1 Design objectives, closed-loop structure and controller design method

The objective of closed-loop control is to force an aeroelastic system to behave in a desired manner. For bridges, the controller design aims at disturbance rejection. Acting disturbances should excite the system states or the measured system output as little as possible. In addition to technical feasibility and economic efficiency, the design should fulfil a set of requirements. Due to the occurring instabilities, a certain level of stability is particularly important for aeroelastic systems. This article addresses stabilisation limits of aeroelastic systems when the described flaps are used. In this case it is hence sufficient to design the controller mainly with respect to a specific stability level.

When closing the control loop with a linear proportional controller **K**,

$$\mathbf{u}_{\text{ac}} = -\mathbf{K}\mathbf{x}_{\text{ol}} \tag{29}$$

stability of the closed loop can again be examined by regarding its eigenvalues. To achieve the intended objective, the controller is designed as a function of the system parameter, the mean horizontal wind speed U. The controller gains are calculated for very closely spaced discrete nodes of the wind speed and cubically interpolated afterwards. There is no assumption for the gains in terms of analytical functions. This gain scheduling can be considered as adaptive control with one drawback. As gain scheduling has no feedback of the actual system behaviour, an incorrect schedule cannot be compensated.

The state feedback chosen in Eq. (29) requires information about all system states which are defined in the first part of the article. While measuring all structural states ξ_s and $\dot{\xi}_s$ and actuator states $\mathbf{x}_c$ can be problematic, it is impossible to measure the mathematically introduced aerodynamical states ξ_a. However, state estimators like Kalman filter or Luenberger observer can reconstruct the system state from the output provided that the system is realistically modelled and observable with its output. The design of the state estimator is not dealt with in this article. As a result of the separation theorem, the mentioned estimators do not modify the closed-loop eigenvalues that are based on state feedback.

If – in addition to guaranteeing a specific stability level – there are no further conditions for the controller matrix, the design generally leads to an active controller. It allows for energy input into the system and, when combined with the chosen state feedback, it is the most favourable controller type concerning stabilisation. Output feedback can only produce worse results. Passive controllers can be seen as a special kind of output feedback. For instance, tuned mass dampers, which are also used for stabilisation of aeroelastic systems (Pourzeynali and Datta 2002, Boonyapinyo *et al.* 2007, Ubertini 2010), can be considered as passively controlled, movable masses. Due to their dissipative nature, passive controllers can only perform less effective compared to active ones. Safety aspects of active stabilisation in permanent operation are not contemplated in this article. At least for construction stages of bridges with undesirable aeroelastic characteristics, active controllers are considered to be a useful option.

The chosen linear-quadratic control, which is also called optimal control, reduces the controller design to the minimisation of a quadratic cost functional. This functional includes the states and inputs of the system. In order to simplify the analysis, a different weighting of the states and inputs is not primarily taken into account. A specific level of stability can easily be achieved for optimal controllers. The system matrix is modified by adding ($-\sigma_{\max}$) times the identity matrix. Hence, all eigenvalues of the closed loop are placed to the left of the bound $\sigma_{\max}$ in the complex frequency plane. For the numerical example $\sigma_{\max} = -56.5 \cdot 10^{-3}$ 1/s is assumed.

3.2 Controllability and observability of the extended aeroelastic system

Controllability and observability are basic characteristics of a dynamic system which crucially influence the feasibility of closed-loop control. Only the part of a system that is both controllable and observable can be controlled in a closed loop. These properties can be examined for instance with the Hautus criteria, which are commonly known in control theory. They not only allow statements to be made about the controllability or observability of a system, but also whether a particular eigenvalue has these properties. If controllability or observability only vanish for certain discrete wind speeds, the use of these criteria will be numerically cumbersome because the speeds must be known very precisely. For systems with a single input and a single output, the lack of controllability or observability can be better detected with pole-zero cancellations in the transfer function of the aeroelastic system. For these kinds of systems, transfer zeros become decoupling zeros if controllability or observability vanish. The reduced poles become non-controllable eigenvalues when input decoupling zeros occur and non-observable eigenvalues when output decoupling zeros occur. If the real and the imaginary part of the poles and zeros are graphically displayed against the wind speed, singularities of controllability and observability can be found without difficulty.

When using the Minimum-State Method for approximating the derivatives of motion-induced aerodynamic forces, all eigenvalues of the extended aeroelastic system investigated here – disregarding the a priori excluded eigenvalues of the mathematical actuator – are generally controllable with the chosen input. Exceptions will be described in Section 3.3 . If the output signals are selected appropriately, disregarding again the eigenvalues of the mathematical actuator, the extended system is completely observable as well. For this purpose, the output of the bridge rotation angle α is sufficient for all wind speeds without exceptions.

Another form of the rational approximation according to Roger (1977) and Abel (1979) leads to several non-controllable eigenvalues for all wind speeds in the case of the theoretically described flat plate. Their occurrence can be explained with identical parallel subsystems within the state-space model due to the other way of approximation. The non-controllable eigenvalues are, however, located in the stable, left part of the complex frequency plane and do not need to be stabilised. When using the canonical form of the state-space model, these eigenvalues can be separated. Then the controller can be designed for the controllable part of the system. All results presented here can be derived with this approximation alternative as well. Any associated stumbling blocks are not addressed in this article.

3.3 Properties of the controller matrix

Figs. 4 and 5 show the graphs of one element of the calculated controller matrices that connects the input α_c or $\alpha_{c,lee}$ with the bridge rotation angle α. The behaviour of this element is typical of the controller. When calculating the gains, the algorithm fails at $U = 60.9$ m/s. For this wind speed, the extended aeroelastic system shows the transition from two distinct real to two complex-conjugate eigenvalues (cp. Fig. 3). At the mentioned wind speed there is a double eigenvalue with two identical eigenvectors. A diagonal canonical form of the system matrix does not exist for that case. Numerically, the developed algorithm produces an artefact in the form of a narrow-spaced

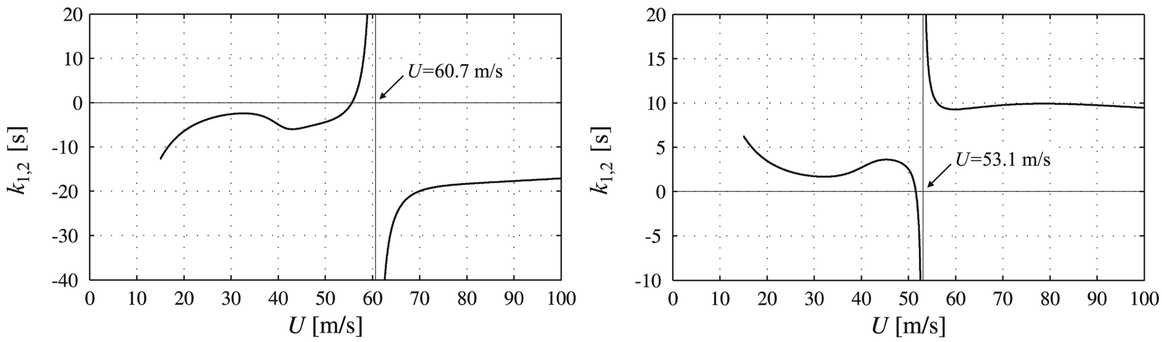

Fig. 4 Controller gains for kinematically coupled flaps; moved in the same direction on the left, moved in opposite directions on the right

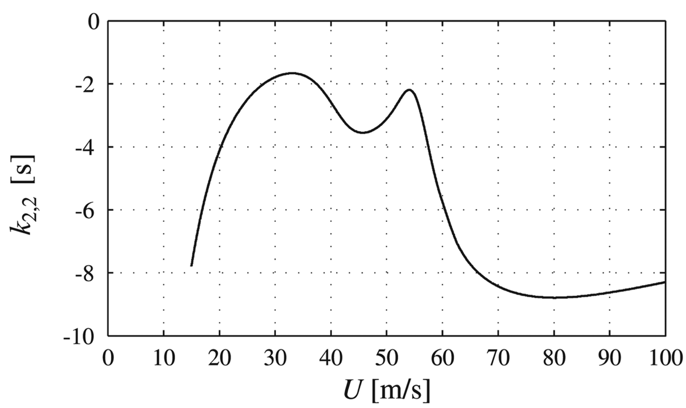

Fig. 5 Controller gain for separately driven flaps

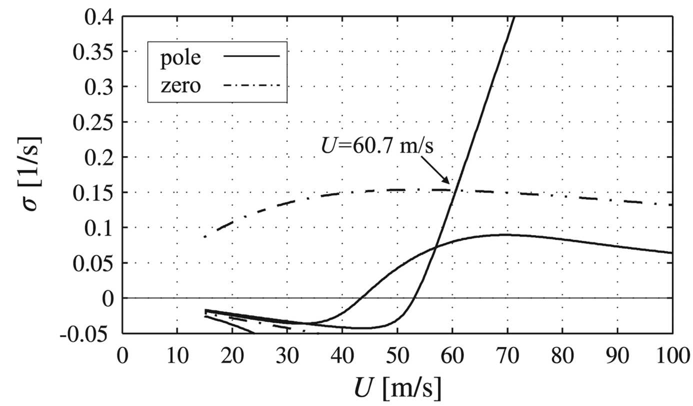

Fig. 6 Real parts of poles and zeros of the transfer function of the aeroelastic system extended with kinematically coupled flaps that are moved in the same direction

pole in the controller gain. The problem can be circumvented by interpolating the results at two wind speeds that are sufficiently far away from the critical point. This has been done before plotting Figs. 4 and 5 .

At $U = 43.5$ m/s, which is the flutter wind speed of the extended aeroelastic system, no distinctive behaviour appears in the controller graph. Therefore, the crossing of the imaginary axis by complex-conjugate eigenvalues constitutes no significant point for the dimensioning of the controller. For kinematically coupled flaps, the controller gain shows a pole-like singularity at another wind speed. This behaviour can be explained when regarding the pole-zero graphs. For flaps that are rotated in the same direction, there is a pole-zero cancellation on the real frequency axis at $\sigma = 0.153$ 1/s for a wind speed of $U = 60.7$ m/s (Fig. 6). As state feedback is chosen, this corresponds to a non-controllable eigenvalue. When moving in the modal shape of the non-controllable eigenvalue, the effect of the generated motion-induced aerodynamic forces is neutralised by the excited structural forces. The non-controllable eigenvalue, which is located in the positive frequency half plane, cannot be stabilised by the controller. When approaching the singularity, the controllability of the aeroelastic system decreases. The controller design algorithm tries to compensate this by increasing the controller gain. The gain thus tends to infinity when the singularity of controllability is reached. The controller values below and above the pole significantly differ in their ordinates. If the kinematically coupled flaps are moved in opposite directions, a pole occurs in the controller gain exactly at the divergence wind speed $U = 53.1$ m/s of the extended aeroelastic system (Fig. 4). The reason is a non-controllable eigenvalue in the origin of the frequency plane. Another explanation can be given as follows. The motion of the flaps produces an additional steady lift force but no additional steady aerodynamic moment. Due to non-existent couplings, the possible modification of the steady translational aerodynamic stiffness has no effect on the steady rotational aeroelastic stiffness that vanishes in the case of divergence. Fig. 5 illustrates that there are no non-controllable eigenvalues or singularities of the controller gain if the flaps are driven separately.

Comparative analyses for control inputs with forces show the same singularities of controllability. For aerodynamic forces of a plate combination with sealed gaps according to Küssner and Göllnitz (1964) and Theodorsen and Garrick (1941) or for hinges that are positioned at the edges of the bridge cross section, there are poles of the controller gain at similar locations as described above. The consideration of a flap mass affects the position of the singularity – concerning the wind speed − only for kinematically coupled flaps that are moved in the same direction. This very small shift is caused by the location of the non-controllable eigenvalue outside the origin of the frequency plane. Edwards (1977) describes similar singularities of controllability for force inputs on the leeward flap.

The non-controllable eigenvalues are not a consequence of poorly approximated aerodynamic forces. The relative difference between the approximated values and the original values is sufficiently small for $s = 0.153$ 1/s. In the origin of the frequency plane, the values of the approximation and the ones of potential theory are identical as it is explained in Section 2.1. When higher, not really realistic levels of damping are chosen for the controller design, further singularities of the controller gain emerge. They are caused by non-controllable eigenvalues on the stable, negative branch of the real frequency axis. These eigenvalues originate from the approximation of the aerodynamic forces with rational functions whose poles create large differences from values of potential theory (Kirch and Peil 2011).

4. Characteristics of the closed-loop system

After inserting the feedback Eq. (29) into the state Eq. (28(a)) of the extended aeroelastic system, the behaviour of the closed-loop-controlled system can be simulated. The dynamic characteristics of

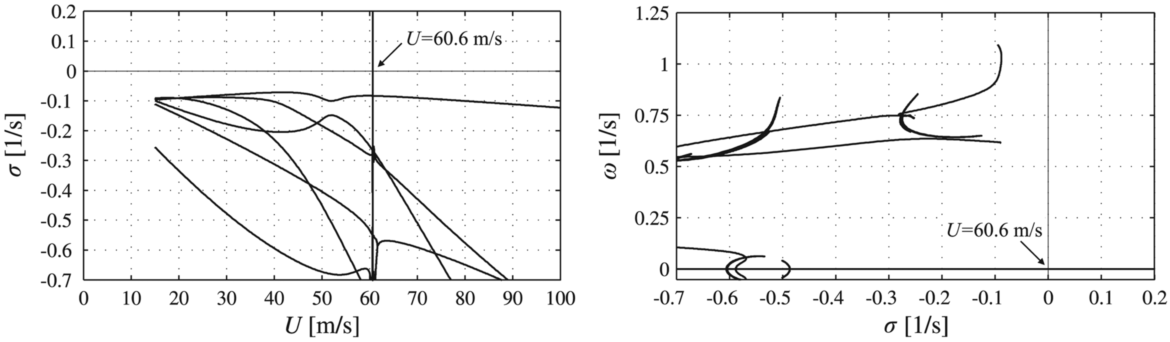

Fig. 7 Eigenvalues of the aeroelastic system controlled with kinematically coupled flaps that are moved in the same direction

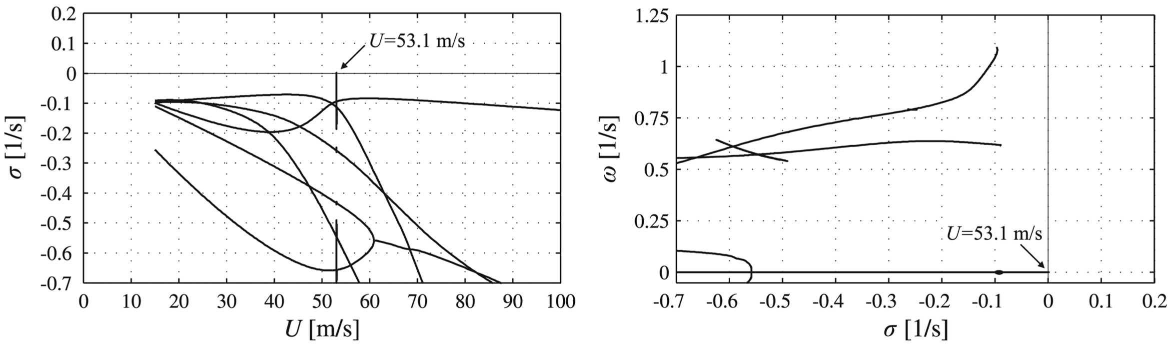

Fig. 8 Eigenvalues of the aeroelastic system controlled with kinematically coupled flaps that are moved in opposite directions

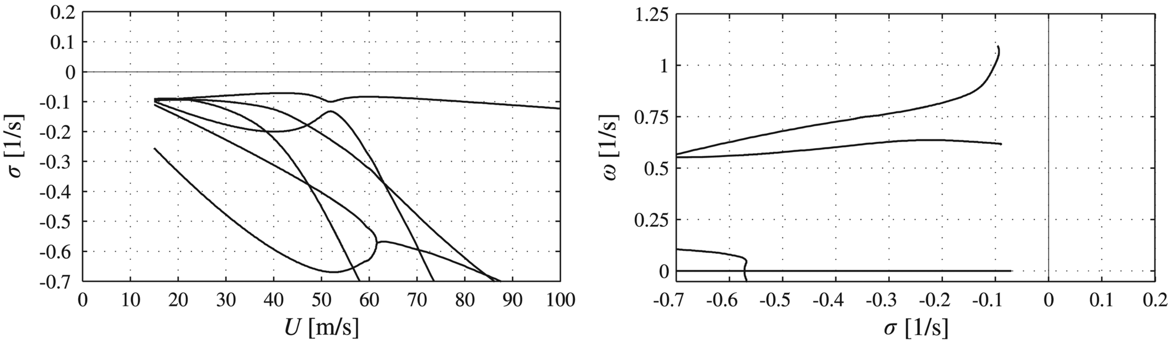

Fig. 9 Eigenvalues of the aeroelastic system controlled with separately driven flaps

the controlled system can again be found with an eigenvalue analysis of its system matrix $\mathbf{A}_{\mathrm{cl}}$.

$$\mathbf{A}_{\mathrm{cl}} = \mathbf{A}_{\mathrm{ol}} - \mathbf{B}_{\mathrm{ol}}\mathbf{K} \tag{30}$$

Figs. 7-9 show the eigenvalues of the closed loops. As expected, the controllers move the low-damped or unstable parts of the curves below the selected level of the frequency real part except for the eigenvalues that are not asymptotically stable and non-controllable. Due to interpolation deficiencies of the controller gain, the instability of the closed loop arises slightly below the wind speed where a non-controllable eigenvalue occurs and disappears slightly above it. Active controllers are able to stabilise the aeroelastic system for all other wind-speed ranges if a linear theory is applied. For both cases of kinematically coupled flaps, system states that are Lyapunov stable but not asymptotically stable appear in the form of an aeroelastic divergence. Fig. 7 shows a divergence wind speed at $U = 60.6$ m/s for flaps that are rotated in the same direction. Concerning its numerical value, this speed is comparable to the divergence wind speed of the flap-free aeroelastic system. For flaps that are rotated in opposite directions, divergence occurs at the relatively low speed of $U = 53.1$ m/s (Fig. 8), which is also the divergence wind speed of the uncontrolled, flap-extended aeroelastic system. Compared to the flap-free system, the critical wind speed is only increased by about 11.6%. Based on this result, coupled flaps that are moved in opposite directions perform distinctly worse than the ones that are moved in the same direction. Close to the points where instability occurs, the loop can be so sensitive that the interpolation causes a noticeable drop below the required damping level. In the right part of Figs. 7 and 8, this lack of robustness causes the noose-like eruptions of the eigenvalue paths. A powerful sorting algorithm for the calculated eigenvalues allows these curves to be determined. For separately driven flaps, there is no instability (Fig. 9). When using a linear theory, the aeroelastic system can be stabilised for all wind speeds by separately driven flaps.

The high feedback gains around the wind speeds at which instabilities of the closed-loop systems occur are effective only to a certain extent for real systems due to the linearisation of the model. Additionally, these theoretically derived wind speeds are associated with uncertainties as a result of modelling errors. In combination with the step-like change of the controller values, the aeroelastic system remains unstable in a non-negligible interval. Even advanced adaptive control strategies with feedback of the system behaviour are likely to fail due to these problems. Based on these explanations, the wind speeds where non-controllable eigenvalues of the flap-extended aeroelastic systems occur must be regarded as an upper limit for the application of kinematically coupled flaps even when using active control.

All results are based on small rotations of the plates. The size of the acting disturbances determines whether the limits that have been found so far can be reached at all. Hence, the behaviour of the aeroelastic system under the influence of gusts will be investigated in the next section.

5. Performance of the controlled system under the influence of a gust disturbance

The gust-induced forces $\mathbf{d}^g$ in the state-state space models of the aeroelastic system have not been specified so far. Using the variables that are introduced and explained in the first part of the article, they can again be described with a state-space model in an elegant way

$$\dot{\xi}_a^g = \mathbf{A}_g \xi_a^g + \mathbf{B}_g \mathbf{a}_g \tag{31a}$$

$$\mathbf{d}^g = \mathbf{C}_g \xi_a^g + \mathbf{D}_g \mathbf{a}_g \tag{31b}$$

where

$$\mathbf{a}_g = (\ddot{\mathbf{a}}_g^T \;\; \dot{\mathbf{a}}_g^T \;\; \mathbf{a}_g^T)^T \tag{32}$$

The matrices of the state-space model can be derived from the matrices of the rational function approximation of the gust admittances as follows.

$$\mathbf{A}_g = \frac{U}{b}\mathbf{R}^g, \quad \mathbf{B}_g = (\mathbf{0} \;\; \mathbf{E}^g \;\; \mathbf{0}), \quad \mathbf{C}_g = q_0 \mathbf{D}^g, \quad \mathbf{D}_g = q_0\left(\left(\frac{b}{U}\right)^2 \mathbf{A}_2^g \;\; \frac{b}{U}\mathbf{A}_1^g \;\; \mathbf{A}_0^g\right) \tag{33}$$

As has been shown in Eq. (27) for the model of the mathematical actuator, the disturbance model can be combined with the models of the aeroelastic system into a single state-space model. For the controlled aeroelastic system, the equations are as follows.

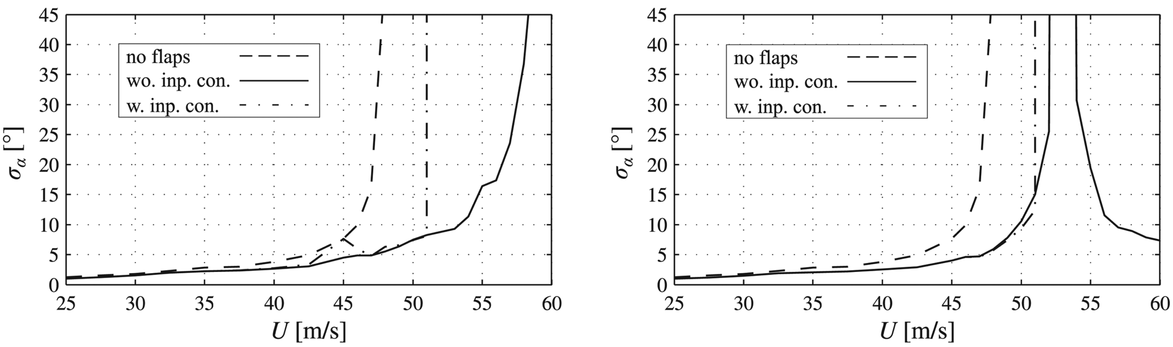

Fig. 10 System responses to a gust disturbance for kinematically coupled flaps; moved in the same direction on the left, moved in opposite directions on the right. (abbr.: w. / wo. inp. con.: with / without input constraints)

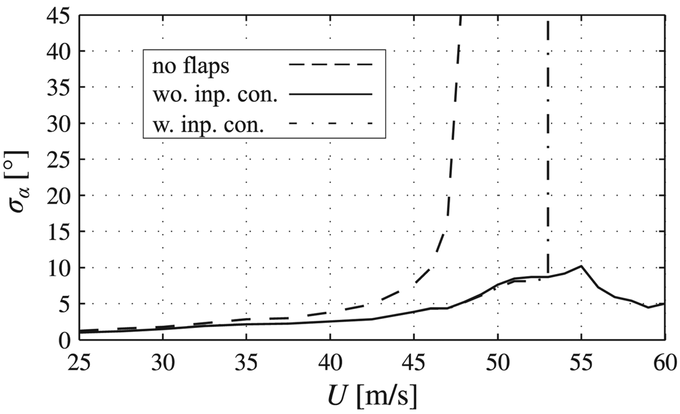

Fig. 11 System responses to a gust disturbance for separately driven flaps (abbr.: w./wo. inp. con.: with/without input constraints)

$$\begin{pmatrix} \dot{\mathbf{x}}_{\mathrm{ol}} \\ \dot{\xi}_{\mathrm{a}}^{\mathrm{g}} \end{pmatrix} = \begin{pmatrix} \mathbf{A}_{\mathrm{cl}} & \mathbf{E}_{\mathrm{ol}}^{\mathrm{g}}\mathbf{C}_{\mathrm{g}} \\ \mathbf{0} & \mathbf{A}_{\mathrm{g}} \end{pmatrix} \begin{pmatrix} \mathbf{x}_{\mathrm{ol}} \\ \xi_{\mathrm{a}}^{\mathrm{g}} \end{pmatrix} + \begin{pmatrix} \mathbf{E}_{\mathrm{ol}}^{\mathrm{g}}\mathbf{D}_{\mathrm{g}} \\ \mathbf{B}_{\mathrm{g}} \end{pmatrix} \mathbf{a}_{\mathrm{g}} + \begin{pmatrix} \mathbf{E}_{\mathrm{ol}}^{\mathrm{d}} \\ \mathbf{0} \end{pmatrix} \mathbf{d}^{\mathrm{d}} \tag{34a}$$

$$\mathbf{y} = (\mathbf{C}_{\mathrm{ol}} \;\; \mathbf{0}) \begin{pmatrix} \mathbf{x}_{\mathrm{ol}} \\ \xi_{\mathrm{a}}^{\mathrm{g}} \end{pmatrix} \tag{34b}$$

The elements of the gust disturbance $\mathbf{a}_{\mathrm{g}}$ can be generated from given spectra in the frequency and the time domain. In the numerical example, the vertical turbulence is described with a v. Kármán spectrum that has a turbulence intensity of $I_{\mathrm{w}} = 0.07$ and an integral time scale of $T_{\mathrm{w}} = 0.75$ s .

The system response to the gust disturbance can be calculated for linear systems in both the frequency and the time domain. Figs. 10 and 11 display the standard deviation σ_α of the bridge-deck rotation of the controlled systems. These graphs are based on sufficiently long time-domain simulations. Additionally, the rotations of the flap-free system are displayed. Especially near the unstable points of the systems that are controlled with kinematically coupled flaps, the rotation angles noticeably increase. In these ranges, the rotations of the girder cross section and particularly those of the flaps have large numerical values that are not realistic. In addition they violate the assumption of small rotations especially for the model of aerodynamic forces. Fig. 11 shows simulation results for the same controller gains as before where the flap rotations are limited to $\alpha_{\mathrm{c,lee}}, \alpha_{\mathrm{c,win}} \leq 20^{\mathrm{o}}$. Under these assumptions, the stabilisation with flaps fails for all cases in the range of $U = 51.0 \div 53.0$ m/s . This wind-speed limit is only $10 \div 15\%$ higher than the comparable one of the flap-free system.

A possible weighting of the states and inputs in the cost function of the optimal controller design primarily causes a reduction of the bridge-girder rotation by larger flap rotations and vice versa. The given statements about the behaviour of the closed-loop system under a gust disturbance qualitatively remain unchanged. A real application of the favourable state feedback requires state estimators. They worsen the results of Figs. 10 and 11. Below $U = 42.0$ m/s , the deflections of the aeroelastic system under the effect of gust disturbances are in some ranges practically not alleviated with flaps when state estimation is taken into account.

6. Conclusions

Unlike their application to aircraft wings, aerodynamically effective control shields are additional components for bridges. They do neither directly bear any live load nor increase the stiffness of the bridge girder. Unintentionally, not only motion-induced aerodynamic forces but also additional gust-induced forces are generated. In this article, flaps are investigated that are attached to both sides of the bridge cross section. Concerning their ability to stabilise bridges under wind action, the following results are obtained in the article for the considered system and the different flap mechanisms: While, under linear assumptions, separately driven flaps can stabilise the bridge at all wind speeds, non-controllable eigenvalues limit the application range of kinematically coupled flaps. For the numerical example used here, the bounds are located between the flutter and the divergence wind speed of the flap-free system. Even active control, which is favourable for stabilisation, cannot overcome these limitations. Concerning their use in the natural, turbulent wind field, all investigated configurations show – with respect to the quality of the model – that the maximum wind speed for the used bridge model can be enhanced by about $10 \div 15\%$. Moreover, flaps do not seem to be a proper tool for effectively suppressing the effects of gusts within the range of application of the flap-free system.

Further theoretical investigations of stabilisation and disturbance rejection of aeroelastic bridge systems with actively controlled flaps should be performed with a more realistic modelling of the flow around the girder for large displacements. This could be done with the help of CFD algorithms that are for instance applied by Ostenfeld and Larsen (1997) and Preidikman and Mook (1997). Additionally, the parameters of the structure and the dimensions of the aerodynamically effective cross-sections should be more systematically varied. The conclusions drawn for section models should, moreover, be checked with three-dimensional models and, if necessary, be modified.

Acknowledgements

We gratefully acknowledge the support given to this work by the International Graduate College IGC 802 of the German Research Foundation (DFG)

References

Abel, I. (1979), *An analytical technique for predicting the characteristics of a flexible wing equipped with an active flutter-suppression system and comparison with wind-tunnel data*, NASA-TP-1367, Technical Paper, NASA.

Aslan, H. and Starossek, U. (2008), "Passive control of bridge deck flutter using tuned mass dampers and control surfaces" EURODYN 2008 - *Proceedings of the 7th European Conference on Structural Dynamics*, Southampton / UK , Paper E298.

Boonyapinyo, V., Aksorn, A. and Lukkunaprasit, P. (2007), "Suppression of aerodynamic response of suspension bridges during erection and after completion by using tuned mass dampers", *Wind Struct*., **10**(1), 1-22.

Cobo del Arco, D. and Aparicio, Á.C. (1999), "Improving suspension bridge wind stability with aerodynamic appendages", *J. Struct. Eng. - ASCE*, **125**, 1367-1375

Edwards, J.W. (1977), *Unsteady aerodynamic modeling and active aeroelastic control*, NASA-CR-148019, Contractor Report, NASA.

Hansen, H.I. (1998), *Active vibration control of long suspension bridges*, Dissertation, Aalborg University, Denmark.

Hansen, H.I., Thoft-Christensen, P., Mendes, P.A. and Branco, F.A. (2000), "Wind-tunnel tests of a bridge model with active vibration control", *Struct. Eng*., **10**(4), 249-253.

Hansen, H.I. and Thoft-Christensen, P. (2001), "Active flap control of long suspension bridges", *J. Struct. Control*, **8**(1), 33-82.

Huynh, T. (2000), *Suspension bridge aerodynamics and active control*, Dissertation, Aalborg University, Denmark.

Huynh, T. and Thoft-Christensen, P. (2001), "Suspension bridge flutter for girders with separate control flaps", *J. Bridge Eng*., **6**, 168–175.

Karpel, M. (1981), *Design for active and passive flutter suppression and gust alleviation*, NASA-CR-3482, Contractor Report, NASA.

Kirch, A. and Peil, U. (2009), "Fundamental restrictions for the closed-loop control of wind-loaded, slender bridges", *Wind Struct*., **12**(5), 457-474.

Kirch, A. and Peil, U. (2011), "Transfer function approximation of motion-induced aerodynamic forces with rational functions", *Wind Struct*., **14**(2), 133–151.

Klein, R.E., Cusano, C. and Stukel, J.J. (1972), "Investigation of a method to stabilize wind induced oscillations in large structures", *Proceedings of the ASME Winter Annual Meeting*, New York, Paper 72-WA / Aut-11.

Kobayashi, H. and Nagaoka, H. (1992), "Active control of flutter of a suspension bridge", *J.Wind Eng. Ind. Aerod*., **41**(1-3), 143–151.

Küssner, H.G. and Göllnitz, H. (1964), *Tabellen der aerodynamischen Derivativa des schwingenden Streckenprofils mit Knicken und Stufen*, DLR FB 64-05, Technical Report, Deutsche Luft- und Raumfahrt. (DLR) (in German).

Küssner, H.G. and Schwarz, L. (1940), "Der schwingende Flügel mit aerodynamisch ausgeglichenem Ruder", *Luftfahrtforschung*, **17**, 337–354 (in German).

Kwon, S.D. (1996), *Flutter analysis and active aerodynamic control of long-span bridges under wind loads*, Dissertation, Seoul National University, Korea.

Kwon, S.D. and Chang, S.P. (2000), "Suppression of flutter and gust response of bridges using actively controlled edge surfaces", *J.Wind Eng. Ind. Aerod*., **88**(2-3), 263-281.

Lunze, J. (2004), *Regelungstechnik 1: Systemtheoretische Grundlagen, Analyse und Entwurf einschleifiger Regelungen*, Ed. 4th, Springer, Berlin (in German).

Lunze, J. (2005), *Regelungstechnik 2: Mehrgrößensysteme, Digitale Regelung*, Ed. 3rd, Springer, Berlin (in German).

Nissen, H.D., Sørensen, P.H. and Jannerup, O. (2004), "Active aerodynamic stabilisation of long suspension bridges", *J. Wind Eng. Ind. Aerod*., **92**(10), 829-847.

Omenzetter, P., Wilde, K. and Fujino, Y. (2000a,b), "Suppression of wind-induced instabilities of a long span bridge by a passive deck-flaps control system - Part I: Formulation; Part II: Numerical simulations" , *J. Wind Eng. Ind. Aerod*., **87**(1), 61-91

Omenzetter, P., Wilde, K. and Fujino, Y. (2002a,b), "Study of passive deck-flaps flutter control system on full bridge model. – I: Theory; II: Results" *J. Eng. Mech. - ASCE*, **128**, 264-286.

Ostenfeld, K.H. and Larsen, A. (1992), "Bridge engineering and aerodynamics", Aerodynamics of Large Bridges, *Proceedings of the 1st International Symposium on Aerodynamics of Large Bridges*, Copenhagen, Denmark, 3-22.

Ostenfeld, K.H. and Larsen, A. (1997), "Elements of active flutter control of bridges", *Proceedings of the IABSE Conference on New Technologies in Structural Engineering*, Lisbon, 683-694.

Piésold, D.D.A. and Corney, J.M. (1999), "Active aerofoil stabilization of cable-supported bridge decks", *Proceedings of the Institution of Civil Engineers - Structures and Buildings*, 134, 67-76.

Pourzeynali, S. and Datta, T.K. (2002), "Control of flutter of suspension bridge deck using TMD", *Wind Struct*., **5**(5), 407-422.

Preidikman, S. and Mook, D.T. (1997), "A new method for actively suppressing flutter of suspension bridges", *J. Wind Eng.Ind. Aerod*., **69-71**, 955-974.

Preidikman, S. and Mook, D.T. (1998), "On the development of a passive-damping system for wind-excited oscillations of long-span bridges", *J. Wind Eng.Ind. Aerod.*, **77-78**, 443-456.
Roger, K. (1977), "Airplane math modelling methods for active control design", *Proceedings of the Structural Aspects of Active Controls , AGARD Conference*, 228, 4-1 - 4-11.
Sears, W.R. (1940), "Operational methods in the theory of airfoils in non-uniform motion", *J. Franklin I.*, **230**, 95-111.
Simiu, E. and Scanlan, R.H. (1996), *Wind effects on structures: fundamentals and applications to design*, Ed. 3rd , Wiley, New York.
Theodorsen, T. and Garrick, I.E. (1941), *Nonstationary flow about a wing-aileron-tab combination including aerodynamic balance*, NACA-TR-736, Technical Report, NACA.
Tiffany Hoadley, S. and Adams Jr., W.M. (1988), *Nonlinear programming extensions to rational function approximation methods for unsteady aerodynamic forces*, NASA-TP-2776, Technical Paper, NASA.
Ubertini, F. (2010), "Prevention of suspension bridge flutter using multiple tuned mass dampers", *Wind Struct.*, **13**(3), 235-256.
Wilde, K. and Fujino, Y. (1998), "Aerodynamic control of bridge deck flutter by active surfaces", *J. Eng. Mech.-ASCE* ,**124**, 718-727.
Wilde, K., Fujino, Y. and Kawakami, T. (1999), "Analytical and experimental study on passive aerodynamic control of flutter of a bridge deck", *J. Wind Eng.Ind. Aerod*, **80**, 105-119.
Wilde, K., Omenzetter, P. and Fujino, Y. (2001), "Suppression of bridge flutter by active deck-flaps control system", *J. Eng. Mech.-ASCE*, **127**, 80-89.
ZAERO (2004), *ZAERO - Engineers toolkit for aeroelastic solutions Version 7.2*, Theoretical Manual, ZONA Technology, Inc.

CC

Appendix

The following notation is used in this article. Table 1 defines additional variables.

$\mathbf{f}$	vector of motion-induced aerodynamic forces
$\mathbf{G}$	aerodynamic transfer function or aerodynamic admittance function of motion-induced aerodynamic forces
ξ_s	vector of aerodynamically effective degrees of freedom including or not including the flap rotations
p	reduced complex frequency
β, k	real and imaginary part of the reduced complex frequency
s	complex frequency
σ, ω	real and imaginary part of the complex frequency
U	horizontal mean wind speed
b	half width of the aerodynamically effective bridge cross section without control shields
q_0	factor in the aerodynamic transfer equation
ρ	air density (1.25 kg/m^3)
$\mathbf{Q}$	matrix of aerodynamic derivatives
L, M	motion-induced aerodynamic vertical force and moment acting on the total aerodynamically effective cross section
$M_{c,win}$, $M_{c,lee}$	motion-induced aerodynamic moments acting on the flaps around their hinges

h, α	structural degrees of freedom of the bridge cross section
$\alpha_{c,win}$, $\alpha_{c,lee}$	rotational angles of the flaps relative to the bridge deck
b_c	half width of the flaps
$\mathbf{d}^g$	vector of gust-induced forces
$\mathbf{G}^g$	aerodynamic transfer function of gust-induced forces
$\boldsymbol{\alpha}_g$	vector of dimensionless fluctuating wind velocity components
w_g	fluctuating speed of vertical gusts
$\mathbf{A}_j$, $\mathbf{D}$, $\mathbf{E}$, $\mathbf{R}$	matrices of the rational function approximation of the derivatives of motion-induced aerodynamic forces
$\mathbf{I}$	identity matrix
γ_l	elements on the main diagonal of $\mathbf{R}$
n_L	order of the square matrix $\mathbf{R}$ and total number of poles for the rational function approximation
ξ_a	vector of aerodynamic states of motion-induced aerodynamic forces
t, $\bar{t}$	time and non-dimensionalised time
$\mathbf{M}_s$, $\mathbf{C}_s$, $\mathbf{K}_s$	structural matrices of mass, viscous damping and stiffness
$\mathbf{x}$, $\mathbf{y}$	state vector and output vector of the state-space model
$\mathbf{u}$, $\mathbf{d}^d$	vectors of the control input and other disturbance forces
$\mathbf{A}$, $\mathbf{C}$	system matrix and output matrix of the state-space model of the aeroelastic system
$\mathbf{B}$, $\mathbf{E}^g$, $\mathbf{E}^d$	input matrices relating to control input, gust forces and other disturbance forces
$\overline{\mathbf{M}}$, $\overline{\mathbf{C}}$, $\overline{\mathbf{K}}$	matrices of mass, viscous damping and stiffness including aerodynamic effects
ξ_c	displacement inputs
$\mathbf{Q}^s$, $\mathbf{Q}^c$	submatrices of the derivatives corresponding to the structural degrees of freedom and the displacement inputs
$\mathbf{A}_j^s$, $\mathbf{D}^s$, $\mathbf{E}^s$, $\mathbf{R}^s$	submatrices of the rational function approximation corresponding to the structural degrees of freedom
$\mathbf{A}_j^c$, $\mathbf{D}^c$, $\mathbf{E}^c$, $\mathbf{R}^c$	submatrices of the rational function approximation corresponding to the displacement inputs
ξ_a^s, ξ_a^c	vectors of aerodynamic states corresponding to the structural degrees of freedom and the displacement inputs
$\mathbf{A}_c$, $\mathbf{B}_c$, $\mathbf{C}_c$, $\mathbf{D}_c$	matrices of the state-space model for the transfer from displacement inputs to control forces
$\mathbf{x}_c$	input vector of the state-space model for the transfer from displacement inputs to control forces
$\tilde{\mathbf{B}}$	input matrix of the combined state-space model with displacement inputs
$\mathbf{A}_{ac}$, $\mathbf{B}_{ac}$	matrices of the state equation of the mathematical actuator
$\mathbf{u}_{ac}$	displacement input of the mathematical actuator
$\mathbf{C}_a^j$	submatrices of the system matrix of the mathematical actuator
$c_{a,l}^j$	elements of the submatrices $\mathbf{C}_a^j$
$G_{ac,l}$	transfer function from one element of $\mathbf{u}_{ac}$ to the corresponding one of ξ_c
α_c	variable for kinematically coupled flap rotations
$\mathbf{A}_{ol}$, $\mathbf{C}_{ol}$	system matrix and output matrix of the combined state-space model including the model of the mathematical actuator

$\mathbf{B}_{ol}$, $\mathbf{E}_{ol}^{g}$, $\mathbf{E}_{ol}^{d}$	input matrices of the combined state-space model including the model of the mathematical actuator
$\mathbf{x}_{ol}$	state vector of the combined state-space model including the model of the mathematical actuator
$\mathbf{K}$	matrix of feedback gains
σ_{max}	intended maximal value of the eigenvalue real parts of the controlled system
$\mathbf{A}_{cl}$	system matrix of the controlled system
$\mathbf{A}_{g}$, $\mathbf{B}_{g}$, $\mathbf{C}_{g}$, $\mathbf{D}_{g}$	matrices of the state-space model of gust-induced forces
$\mathbf{a}_{g}$	input vector of the state-space model of gust-induced forces
$\mathbf{A}_{j}^{g}$, $\mathbf{D}^{g}$, $\mathbf{E}^{g}$, $\mathbf{R}^{g}$	matrices of the rational function approximation of the transfer function of gust-induced forces
ξ_{a}^{g}	vector of aerodynamic states of the rational function approximation of the transfer function of gust-induced forces
I_{w}	turbulence intensity
T_{w}	integral time scale
σ_{α}	standard deviation of the rotation α
j, l	matrix and vector indices
$(\,)^{T}$	transposition
$(\dot{\,})$, $(\,)'$	generalised differentiation with respect to the time t and the non-dimensionalised time $\bar{t}$
●——○	Symbol connecting corresponding time (○) and frequency-domain (●) descriptions
i	imaginary unit; $i^{2} = -1$
win, lee	indices for windward and leeward variables